Conformational Study on Sol−Gel Transition in Telechelic Polyelectrolytes Solutions

Ran Zhang,[†,‡] Tongfei Shi,[*,†] Lijia An,[*,†] Zhaoyan Sun,[†] and Zhen Tong[§]

State Key Laboratory of Polymer Physics and Chemistry, Changchun Institute of Applied Chemistry, Chinese Academy of Sciences, Changchun 130022, P. R. China, Graduate University of the Chinese Academy of Sciences, Beijing, 100049, P. R. China, and Research Institute of Materials Science, South China University of Technology, Guangzhou, 510641, China

Received: September 25, 2009; Revised Manuscript Received: February 5, 2010

A special kind of associating polyelectrolytes, telechelic polyelectrolytes, composed of a flexible linear polyelectrolyte and short hydrophobic blocks at both ends, is investigated by means of Monte Carlo simulations in aqueous media. It is found that the interplay between hydrophobic attraction and the long-range electrostatic interaction as well as the counterion distribution exerts a major influence on the chain conformations (two basic conformations: loop and nonloop), association behavior (loop association contributes to loop conformation; free, dangling, and bridge chains contribute to nonloop conformations), and the forming of clusters. At a concentration close to the overlapping concentration ϕ^*, the clusters are found to be further connected by bridge chains under strong hydrophobic interaction, forming a 3D network. In addition, increasing Coulombic interaction strength is in favor of the formation of a gel network. With increasing Coulombic interaction strength, first chains tend to extend and then tend to collapse due to the screening originating from the counterion condensation layer.

1. Introduction

Telechelic ABA triblock copolymer (TTC), containing hydrophobic short blocks at both ends, can associate into structures like micelles and physical networks in aqueous media, which gives it many potential applications from controlled drug release to rheological modifications.[1–7] Recently, considerable interest has been paid to the gelation behavior of TTC. Compared with the neutral TTCs, the charged TTCs, namely, telechelic polyelectrolytes (TPs), will ionize into polyions and their counterions when dissolved in water, whose properties strongly depend on pH and salt addition. The PH-tunable property gives its wider applications in drug delivering and targeting.[5–7] However, the gelation behavior of the TPs with charged blocks is beyond our knowledge.

In the experimental work, scattering techniques including small-angle neutron scattering (SANS), small-angle X-ray scattering (SAXS), laser light scattering (LLS), and dynamic light scattering (DLS), in conjunction with rheological techniques, have been frequently applied to explore the gelation process of charged TTCs.[8–15] The scattering technology can give more information on the association behavior, and the rheological measurement can define the gel point and give the phase diagram. To our knowledge, more attention has been paid to the TPs these days: Tsitsilianis et al.[12] studied the viscoelastic properties of physical gels formed by associative TPs; using scattering and rheology methods, Buhler et al. investigated the phase behavior of hydrophobically modified chitosans (HMCs) in aqueous solution and observed four regions on the phase diagram;[13] with atomic force microscopy (AFM) equipment, Tsitsilianis et al. explored the self-organization of newly synthesized TPs in aqueous media[14] and found two types of associates (end-to-end linear associates and starlike "hairy" loose aggregates); the pH-tunable rheological properties of the TPs were also investigated.[15] Although the gelation of TPs has recently been widely experimentally studied, it is not easy to accurately describe the sharp transition of the sol−gel transition process. Investigating the sol−gel transition on a microscale will be helpful for understanding the physical gelation mechanism.

Theory and simulation have been proven to be powerful methods to investigate association behavior of neutral polymers[16–20] and charged block polyelectrolytes.[21–26] The properties (thermoreversible gelation and phase separation) of neutral ones were well understood by considering the competition of attraction of associating groups (stickers), repulsion caused by excluded volume interaction of monomeric units, and translational entropy of the chains.[26] When polyelectrolytes are involved, the situation gets more complicated: the competition between the attraction of hydrophobic groups and the repulsion of chains with charges located on their soluble blocks, the distribution of counterions in aggregated chains and outer solution, and pH and ionic strength changes due to additional salts or surfactants are all important factors demanding careful consideration. Computer simulations such as molecular dynamics (MD) and Monte Carlo (MC) methods can directly provide specific information such as chain conformation, microscopic structure of physical gels, etc., while this is difficult to determine experimentally. Self-consistent-field (SCF) models and numerical simulations[26] can also provide useful information. Theoretically, when the attraction energy exceeds a thermal energy k_BT, $\varepsilon_{attr} \gg k_BT$, the TP chains can associate into 3D networks in the aqueous solution very close to the overlapping concentration (ϕ^*), while in dilute solutions, these copolymers will form clusters of optimum size.[26] Potemkin et al. also found that the stabilization of these clusters relies on the attraction energy of

* To whom correspondence should be addressed. E-mail: tfshi@ciac.jl.cn (T.S.); ljan@ciac.jl.cn (L.A.). Tel.: +86-431-85262137. Fax: +86-431-85262969.

[†] Changchun Institute of Applied Chemistry, Chinese Academy of Sciences.

[‡] Graduate University of the Chinese Academy of Sciences.

[§] South China University of Technology.

10.1021/jp9092404
Published on Web 02/22/2010

end blocks and the Coulomb interaction together with the contribution from the translational entropy of counterions.[25]

Although the earlier studies give some aspects of sol−gel transition of associating polyelectrolytes, few reports focus on conformation and association behavior during sol−gel transition. As for TP chains, the hydrophobic attraction of end groups has a tendency to fold back the chain, while the repulsion from middle charged blocks tends to stretch the chain. Therefore, the conformation of the TP chains in dilute solution might experience a transition from loop to nonloop due to the increase of the electrostatic repulsion or the decrease of hydrophobic interaction. In fact, there is different association behavior: free, dangling, loop, and bridge, among which loop association contributes to loop conformation whereas the others contribute to nonloop conformation. There are no reports on the effect of the competition of hydrophobic attraction and electrostatic repulsion on conformation transition and association transition. Here, using the off-lattice Monte Carlo techniques, we carried out work on TPs in aqueous solution close to the overlapping concentration (ϕ^*) where the TPs develop into 3D networks under proper hydrophobic and electrostatic conditions. To describe the chain conformations and association behavior during the sol−gel transition, we first studied the percolation phenomena and obtained the phase diagram of the sol−gel. Then we probed the chain conformation, association, and their contribution to sol−gel transition, followed by the investigation of the distribution of cluster size and the distribution of counterions. Finally, we investigated the effect of Coulombic strength on the chain conformations and the gelation behavior. Concluding remarks are presented in the last section.

2. Model and Simulation Details

2.1. Model. In our model system, the telechelic polyelectrolytes are simulated as chains of hard spheres with diameter σ, which is the unit length in this paper. The telechelic polyelectrolyte $A_{N_A} - B_{N_B} - A_{N_A}$ contains 20 monomers, with $N_A \equiv 1$ and $N_B \equiv 18$, where the A block stands for the hydrophobic groups and the B block is a flexible hydrophilic polyelectrolyte, negatively charged. The bond length is fixed at 1.1σ. The solvent is implicitly treated as a dielectric continuum. Counterions are monovalent and positively charged hard spheres with the same diameter as the monomer of the chains. The number of counterions N_c equals the number of charged B monomers, maintaining the charge neutrality. This choice of simulation model is mostly based on the practical consideration of the TPs. The simulation is carried out in a cubic cell ($L = 48\sigma$) with periodic boundary conditions in all directions. The attraction potential between hydrophobic monomers U_{attr} is an attractive Lennard-Jones potential

$$U_{attr} = 4\varepsilon_{attr}\left[\left(\frac{\sigma_{attr}}{r}\right)^{12} - 2\left(\frac{\sigma_{attr}}{r}\right)^{6}\right] \quad (1)$$

where ε_{attr} is the association energy. The interaction between B monomers and other pairs U_{rep} is the repulsive L-J potential

$$U_{rep} = 4\varepsilon_{rep}\left(\frac{\sigma_{rep}}{r}\right)^{12} \quad (2)$$

where ε_{rep} is the repulsive energy. Here $\sigma_{attr} = \sigma_{rep} = \sigma = 1$, and the cutoff of these L-J interactions is 2.5σ. The Coulombic sum of a system $U_{elec,tot}$ with N charges in the main box under periodic boundary condition is given by

$$U_{elec,tot} = k_B T \lambda_B E_{tot} \quad (3)$$

$$E_{tot} = \frac{1}{2}\sum_{\vec{n}}{}' \sum_{i,j}^{N} \frac{q_i q_j}{|r_{ij} + \vec{n}L|} \quad (4)$$

$$\lambda_B = \frac{e^2}{4\pi\varepsilon_o\varepsilon_r k_B T} \quad (5)$$

where k_B is the Boltzmann constant, T refers to temperature, and the Bjerrum length λ_B is defined as the distance at which two unit charges have the interaction energy $k_B T$. λ_B can be considered as a measure of the strength of electrostatic interactions vs the thermal energy and is equal to 7.14 Å for water at room temperature. The symbol $'$ in eq 4 denotes that we omit the term $i = j$ for $\vec{n} = \vec{0}$. In eq 5 e is the elementary unit charge, and $q_{i,j}$ are charges measured in the unit of e. ε_o and ε_r are the relative dielectric constants of the vacuum and the solvent (water), respectively. More details about the Coulombic sum in a MC simulation is given in the Appendix.

2.2. Simulation Details. The MC simulation was performed in the NVT (constant particle numbers, constant volume and temperature) ensemble according to the Metropolis algorithm. A counterion randomly moves in a sphere of diameter $D = 10\sigma$ according to an elementary movement of MC. To relax the chains efficiently and accelerate the convergence of energy, several algorithms like pivot, crankshaft, kink-jump, and translation were used. In a pivot move, a chain node is chosen at first, splitting a chain into halves, and then the shorter part moves around the chosen node; in a translation, the shorter part just takes an even move without breaking the bond connecting the node. Crankshaft and kink-jump are very much alike in pattern: we define an axis by two unconnected nodes in a chain and let the nodes between the chosen ones move around the axis. The main difference between these two methods is that in a kink-jump only one node is moving.

When Coulombic strength ξ ($\xi = \lambda_B/\sigma$) is larger than 1, Manning condensation is reached, and the algorithms above become inefficient due to the counterions located very close to the chain. To solve this problem, "clothed moving algorithms" were used. For instance, in a pivot algorithm, when a part of the chain is chosen, the counterions around it at a distance less than d_s move with the part of the chain.[27] Here, the scale d_s used was optimized to be 2.5σ in our simulation.

3. Simulation Results

3.1. Gelation Process. The percolation model is widely used to determine whether gel is formed or not. However, the percolation model is valid for the criteria of gelation only when the attraction energy ε_{attr} is much higher than $k_B T$.[28,29] Here we set ε_{attr} much larger than $k_B T$. Thus we could apply the percolation model to determine the formation of the gelation. In our simulation $\varepsilon = \varepsilon_{attr}/k_B T$. As ε increases (caused by temperature changes, different species, or fraction of hydrophobic groups), a sol−gel transition is witnessed. For instance, relationship between the percolation probability and ε at concentration 0.0181 is shown in Figure 1a. The solid line is a sigmoidal-Boltzmann fitting curve to the simulation data points. According to Figure 1, the percolation remains zero when $\varepsilon \leq 5.5$, which suggests the system is in the sol state; when $\varepsilon \geq 8$, the system is in the gel state because percolation probability $P(\varepsilon)$ is 100%. Thus, when $5.5 \leq \varepsilon \leq 8$, the system is in the sol−gel state because the percolation probability is between 0 and 1.

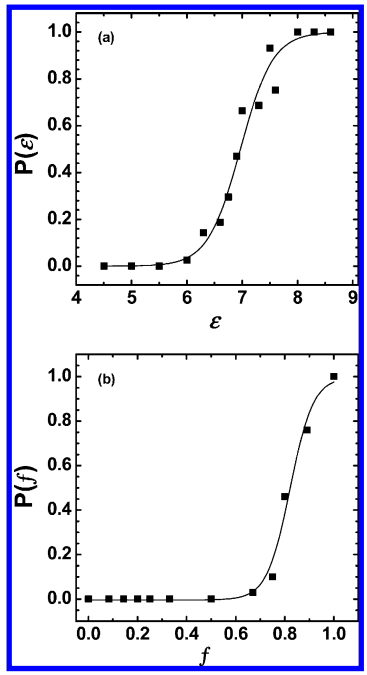

Figure 1. (a) Percolation probability (P) plotted against the hydrophobic interaction energy ε; (b) percolation probability as a function of the charging fraction f. Coulombic strength is fixed at $\xi = 0.5$. The solid line is the sigmoidal-Boltzmann fit of the percolation data.

According to the above results, TPs can form a 3D network at very low concentration (just above the overlap concentration ϕ^*). However, it is known that neutral telechelic polymer cannot do so at such low concentration.[30] In order to understand why the electrostatic interaction involved in TPs makes its gelation much different from neutral telechelic polymer, we investigate the charging fraction effect of the middle block on gelation and conformation. We uniformly charge/discharge the middle polyelectrolyte blocks every n ($n = 1, 2, 3, \ldots$) monomers and acquire TPs charging fraction f from 100% to 0; here we set $\varepsilon = 8$, which ensures the hydrophobic interaction enough for the 100% charged system to form a gel. Figure 1b shows that the percolation $P(f)$ drops quickly after the TPs are discharged. It is found that the percolation value remains zero and the system stays in a sol state when $f < 0.6$. This indicates that the TP system is losing its ability of forming a 3D network structure with the decrease of f. Figure 2 is the snapshots of simulation under fully charged and noncharged conditions at $\varepsilon = 8$. It is obvious that for a 100% charged system, the network structure is obviously formed. Some of the chains are fully extended by electrostatic repulsion and connect the separated hydrophobic bundles. However, for the noncharged system, the hydrophobic end groups only make the chains aggregate into some separate clusters with "collapsed" structure compared with the 100% charged system and fail to associate the chains to form a 3D network. Therefore, at such a low concentration, without the strong support of electrostatic repulsion, chains may not be prone to stretch and connect different clusters so that chains fail to hold a spacial structure. Further investigation of conformations with the variation of charging fraction will be helpful for understanding the effect of the electrostatic interaction, which will be discussed in the following section.

3.2. Chain Conformations and Association Types. Based on the above discussion, we know that the gelation of TPs at this low concentration is attributed to the combination of hydrophobic attraction in the short-range and the electrostatic repulsion in the long-range. In fact, the interplay between hydrophobic attraction and the electrostatic repulsion will influence the conformation. In our system, the hydrophobic ends (A block) will gather together to form a bundle. If the both ends in the same chain are in the same bundle, the conformation is a loop conformation. Thus, there are two main conformations, loop and nonloop. It is unclear that the chain conformations evolve during the gelation process.

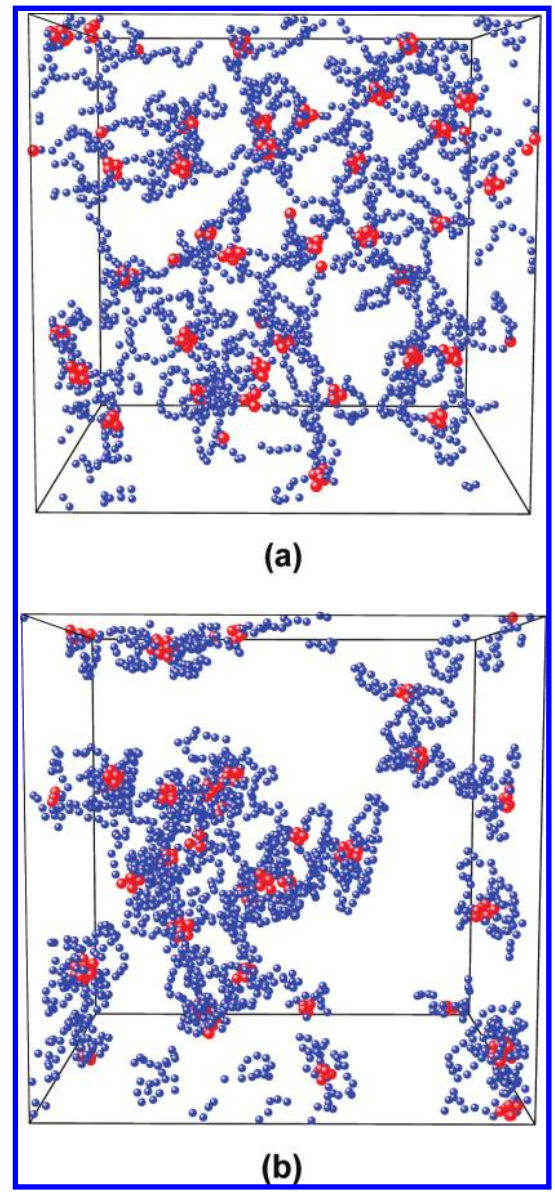

Figure 2. Snapshots of simulation at $\varepsilon = 8$, $\xi = 0.5$: (a) 100% charged; (b) a neutral telechelic system. The hydrophobic end groups are shown in red, and the middle block is shown in blue.

To clearly understand the electrostatic repulsion effect, we first investigate the relation between charging fraction and conformation. Figure 3 shows the fraction of loop conformation and the radius of gyration vs charging fraction, respectively. Figure 3a shows that the fraction of loop chains increases from less than 60% to almost 80% by discharging. The radius of gyration of TP chains decreases from about 3.2σ to less than 2.6σ with the decrease of charging fraction (see Figure 3b). Therefore, the chains tend to shrink and form the loop conformation with the reduced electrostatic repulsion. Thus, when the charging fraction f equals zero (namely, neutral telechelic polymers), the system is in a sol state because nonloop chains are not enough to connect clusters into a 3D network in such low concentration.

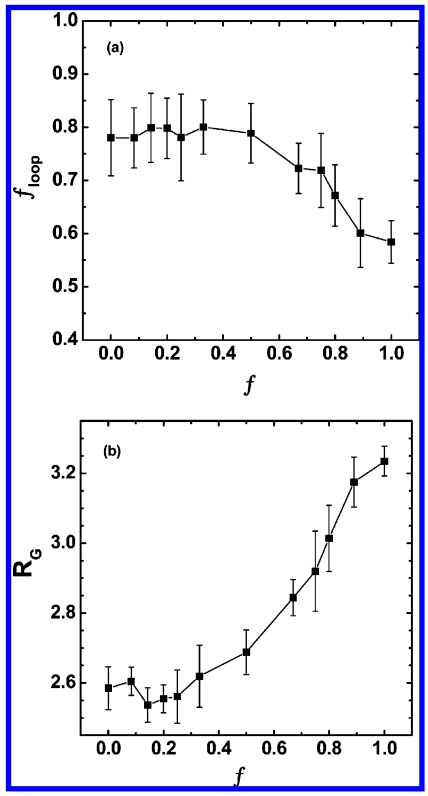

Figure 3. (a) Fraction of loop conformation f_{loop} plotted against the charging fraction f; (b) the radius of gyration R_G plotted against f.

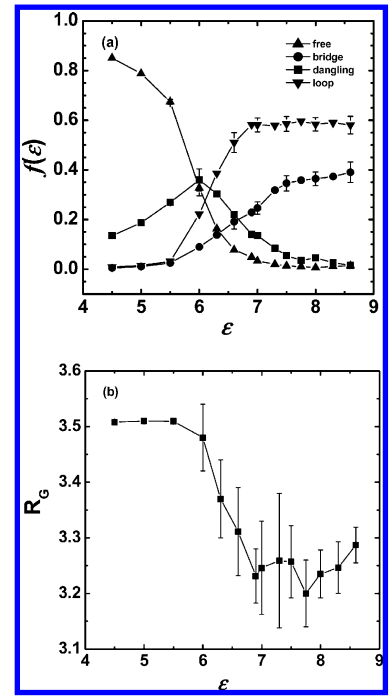

Figure 4. (a) Chain association type fraction as a function of the hydrophobic interaction energy ε for a fully charged system with a Coulombic strength $\xi = 0.5$; (b) the radius of gyration R_G plotted against ε.

Compared with the neutral telechelic polymers, TPs can undergo the gelation at the very low concentration close to the overlap concentration because of not only the relative strong hydrophobic attraction but also the electrostatic repulsion among monomers. It is obvious that loop conformation is from the loop association behavior, which makes both hydrophobic ends into different bundles. However, nonloop conformation is from the contribution of free, dangling, and bridge chains according to Tanaka's work;[31] **bridge** chains connect different bundles into **clusters**; a **dangling** chain buries one end into the bundle and extends the other into the aqueous media, ready to become a loop or bridge; a **free** chain keeps both ends isolated, swimming alone in the solution. Thus, it is necessary to investigate the different association behavior during sol−gel transition so as to understand the relation between conformation and gelation in a deep way.

To understand the association behavior, we introduce $f(t, \varepsilon)$, the fraction of t type of chains. Figure 4a shows $f(t, \varepsilon)$ as a function of hydrophobic attraction ε. When $\varepsilon \leq 5.5$, the system is in the sol state. f(loop, ε) and f(bridge, ε) are very low, nearly zero. This indicates that TPs in solution maintain a nonloop conformation mainly composed of free and dangling types due to the relatively weak hydrophobic attraction in comparison with the long-ranged electrostatic repulsion. In addition, f(free, ε) is very large and decreases with ε while f(dangling, ε) increases. This implies that some free chains change into dangling chains with increasing ε by aggregating into starlike micelles. When $5.5 < \varepsilon < 6.0$, it starts to be in the sol−gel state. f(free,ε) decreases sharply and others increase with ε. According to our previous model, the dangling chain serves as an intermediate.[30] Namely, free chains change into loop chains and bridge chains via dangling chains. Thus, many free chains transform into dangling chains and some dangling chains transform into loop chains to result in a conformation transition or into bridge chains to act as a connection between bundles. In this range of ε, it is obvious that dangling chains change into loop chains more than bridge chains. In addition, dangling chains obtained from free chains are more than those changing into loop chains and bridge chains due to f(dangling, ε) increasing with ε. Furthermore, f(dangling, ε) reaches a maximum at $\varepsilon \approx 6.0$ and then decreases with ε. The maximum is attributed to the competition of two transformations, free chains into dangling chains and dangling chains into loop and bridge chains. Increasing ε leads to more hydrophobic ends into bundles, which balances the repulsive electrostatic interaction between charged monomers, entropy penalty of the translational counterions, and hydrophobic interaction. The picture shows that f(loop, ε) increases with ε more quickly than f(bridge, ε). This indicates both hydrophobic ends from the same chains insert the same bundles more than in the different bundles. After $\varepsilon \approx 7.0$, f(loop, ε) is nearly independent of ε but f(bridge, ε) still increases. The chain conformation transition (from nonloop to loop conformation) reach a balance, but the exchanges of subdivided nonloop types go on. This implies that the forming of loops accumulates the repulsive electrostatic energy to an utmost extent by folding back the charged chains, and further increasing loop chains will lead to the unbalance of electrostatic and hydrophobic interactions. However, TPs can stretch chains to balance the electrostatic repulsion and the hydrophobic attraction by inserting both of their ends into different bundles. After $\varepsilon \approx 8$, the gelation progress is completed. Few free and dangling chains remain in the system, and f(bridge, ε) shows no pronounced changes due to nearly no dangling chains.

Figure 4b show that the radius of gyration R_G drops from nearly 3.5σ to around 3.2σ during the physical gelation process. Its trend corresponds to the f(loop, ε) in a reverse way, since the back-folding of chains into loops reduces their size. When the gelation process is complete, there are mainly two types of chains, the loop and the bridge chains. All the association types contribute to the gelation forming, but apparently the bridge does the most effective part to join up the separated bundles

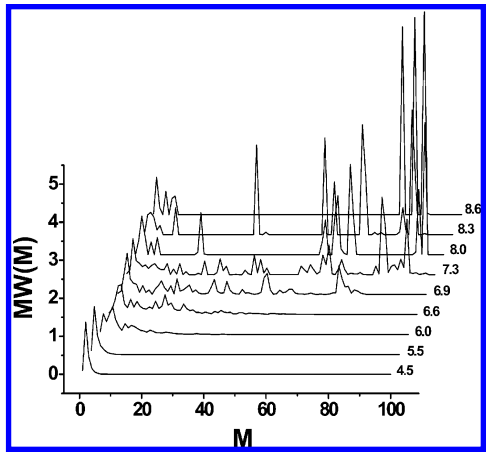

Figure 5. Distribution of clusters with different ε at $\xi = 0.5$; the cluster distribution function $W(M) = N(M)/[N(1) + N(2) + \ldots + N(N)]$, where $N(M)$ is the number of cluster size M.

and clusters. The loops, however, contribute in an indirect way by accumulating the electrostatic repulsion to hold up the spacial structure.

3.3. Aggregation Structures. In order to further understand the relationship between microscale conformation and macroscale gelation, aggregation structures were investigated. From the discussion above we know that changing hydrophobic interaction leads to the transition among different chain types. Chains associate into small bundles or clusters before a 3D network is formed. Figure 5 shows the distribution of cluster size at different ε. It is obvious that cluster size and its distribution strongly depend on ε. When $\varepsilon \leq 5.5$, the cluster size is small and its distribution is homogeneous in the sol state. When $5.5 < \varepsilon < 8$, cluster size exhibits wide distribution during sol−gel transition. When $\varepsilon \geq 8$, the cluster size has two extreme distributions, very large or very small, but most of chains are composed of large clusters rather than small ones. Thus the gel state is formed, which arouses the distribution of cluster size to be narrower instead of wider.

The association types of chains and cluster distribution are briefly understood according to the above results. However, until now we cannot answer the correlation among monomers A, B and the counterions, which is required for further understanding the aggregation structure. Therefore, we investigate their pair correlation functions (see Figure 6). In Figure 6a, the strong peak at $r \approx 1$ comes from the monomers A and B connected by a covalent bond. The peaks in the short-range appear with increasing ε, representing the middle charged monomers packed in an ordered way around the hydrophobic bundles; the peak in the long-range represents the correlation between bundles in the system. Figure 6b is the pair correlation function of the monomers; it is characterized by the peaks in the short-range and in the long-range, indicating that the TP chains correlate with each other in the long-range ($r \approx 10$) when the hydrophobic interaction is weak, and with increasing ε this correlation peak shifts to a longer range ($r \approx 15$) and starts to stand for the correlation between associated micelles.

In our simulation, the monovalent counterions are considered explicitly. Counterions confined near the charged monomers can bring down the Coulombic interaction potential accumulated by the aggregation of negatively charged chains. Figure 6c illustrates the counterions distributing around the hydrophobic end groups. As ε increases, more counterions are confined within the corona of the micelles to stabilize chains carrying negative charges. Figure 6d is the pair correlation function for the

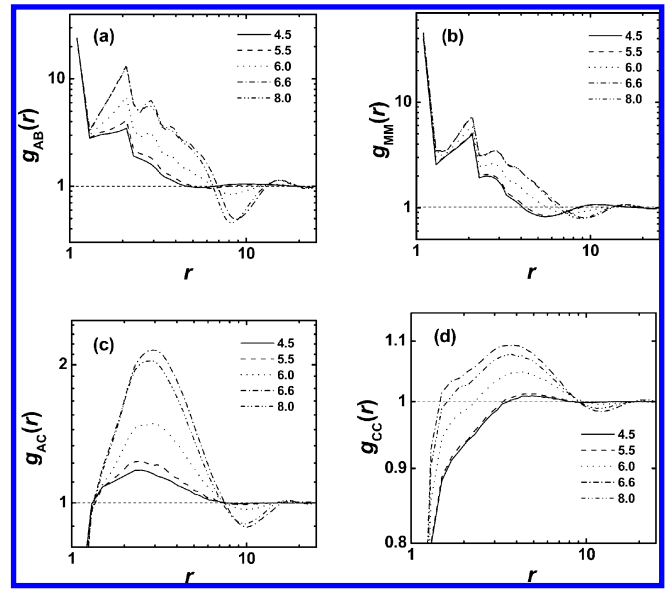

Figure 6. Pair correlation functions $g(r)$ for different components in the system: (a) A(hydrophobic end)−B(polyelectrolyte block), (b) monomer−monomer, (c) A−C(counterion), (d) counterion−counterion.

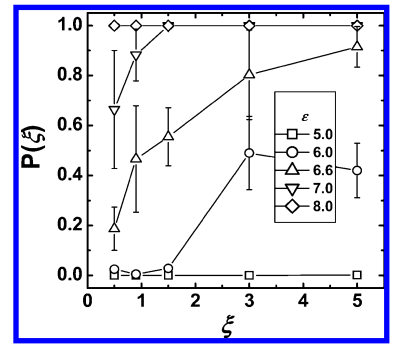

Figure 7. Percolation probability (P) plotted against the Coulombic interaction strength ξ.

counterions. With small ε, the equally charged ions repel each other and g_{cc} remains below 1 at small distance ($r < 3$). Energetically, counterions will have to keep closer to the charged monomers as aggregation develops with increasing ε, so g_{cc} increases with ε in the short-range. This increase of g_{cc} in the short-range suggests that counterions are slightly condensed around the charged monomers. g_{ac} and g_{cc} initially increase with the increase of ε but decrease at $\varepsilon = 8$ when the physical gelation develops completely (see Figure 6c and 6d). This decrease is because the clusters are further connected by bridging chains under the strong hydrophobic interaction and a continuous structure is created, which, to a certain extent, mitigates the inhomogeneous distribution in the system.

3.4. Coulombic Strength. When the Bjerrum length exceeds the so-called Manning critical value (the Coulombic strength $\xi > 1$), counterions are anticipated to form a thin condensation layer around the surface of the charged monomers according to the counterion condensation theory proposed by Manning and Oosawa.[32,33] Apparently, the forming of a gel is also affected by the changing of ξ. Figure 7 shows the percolation behavior with Coulombic strength ξ for different hydrophobic energies. For very weak attraction $\varepsilon = 5$, the percolation probability is 0 and independent of ξ. The system is always in the sol state. For $\varepsilon = 6.0$, percolation probability is 0 and independent of ξ when $\xi \leq 1.5$; after $\xi = 1.5$, further increasing ξ leads to the increase of percolation probability, but an unusual decrease of

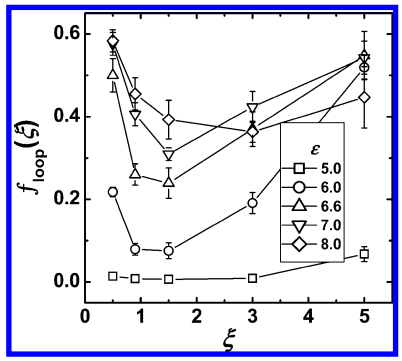

Figure 8. Loop fraction (f_{loop}) plotted against the Coulombic interaction strength ξ.

percolation probability with ξ appears at $\xi = 5.0$. For $\varepsilon = 6.6$ and $\varepsilon = 7.0$, percolation probability increases with ξ at first and then reaches 1. For $\varepsilon = 8$, increasing ξ does not influence the percolation probability because it is always in the gel state.

In order to explain the above percolation results and further understand the effect of Coulombic interaction strength on gel network formation, we investigate the chain conformation first. In fact, increasing the Coulombic interaction strength causes the condensation of counterions around the surface of charged monomers, screening the strong Coulombic interaction. This behavior will affect the equalization formed between the hydrophobic interaction in the short-range and the electrostatic interaction in the long-range, resulting in the change of the chain conformation ratio and the gel formation. For linear polyelectrolytes, the stronger repulsion originating from the charged monomers extends the chain as ξ increases; when $\xi > 1$, counterion condensation occurs, and the chain will collapse due to strong electrostatic interaction.[34] As for TPs, this behavior can be reflected by the fraction of loop conformation formed in the system. Figure 8 shows the loop fraction (f_{loop}) in the system vs Coulombic interaction strength ξ at different hydrophobic interactions ε. For very weak attraction $\varepsilon = 5$, f_{loop} shows no significant dependence on ξ except a slight increase at $\xi = 5$. For larger ε, first, f_{loop} decreases with ξ for the chain is stretched with stronger electrostatic repulsion; then, f_{loop} starts to increase with ξ because further increasing ξ leads to counterions more condensed and the charged monomers effectively screened. At same value of ξ, f_{loop} exhibits an increase in the whole as ε increases. However, for $\varepsilon = 8$ and higher ξ ($\xi > 2$), the increase of f_{loop} does not match our expectation, i.e., f_{loop} gets smaller compared with the cases of $\varepsilon = 6.6$ and $\varepsilon = 7$. This is because the bridge chains benefit from both the stronger hydrophobic interaction and the increasing Coulombic interaction strength, which changes the assignment of chains in conformations.

To interpret our results under the consideration of counterion condensation, the monomer−monomer and the counterion−counterion pair correlation functions are plotted for different Coulombic interaction strength values in Figure 9. If counterions form a condensed layer on the surface of the middle charged block, the counterions themselves should exhibit correlations at certain radial distance in the short-range due to the connectivity of the charged monomers. Figures 9a and 9b show the counterion−counterion pair correlation functions at $\varepsilon = 5$ and $\varepsilon = 8$, respectively. For $\xi < 1$, no obvious peak appears, which indicates that counterions homogeneously distribute. For $\xi > 1$, the peaks in the short-range appear obviously. For instance, at $\xi = 1.5$, there exists a broad peak, which suggests a slight accumulation of counterions, namely, onset of counterion condensation. Increasing ξ makes the peak shift to small r with its height increasing. This implies the counterions are more closely constrained on the surface of monomers. Moreover, Figures 9a and 9b show that at same ξ, this accumulation is more significant at short distance ($r \approx 1.5$) for strong hydrophobic interaction. Figures 9c and 9d show the monomer−monomer pair correlation functions for various Coulombic interaction strengths at $\varepsilon = 5$ and $\varepsilon = 8$. Briefly, the value of the pair correlation functions decreases with the increase of ξ at small distance ($r < 3$), indicating the stronger repulsion between charged monomers. In detail, however, the value of pair correlation functions exhibits a different behavior for $\xi = 3$ and $\xi = 5$. The corresponding plots are similar when $r < 2.2$ but different in the long-range. The reason for the difference is that the counterion condensation around the charged monomers causes electrostatic screening effects to both of them. Therefore, the charged monomers start to effectively attract each other in the long-range when the Coulombic interaction strength is strong enough.

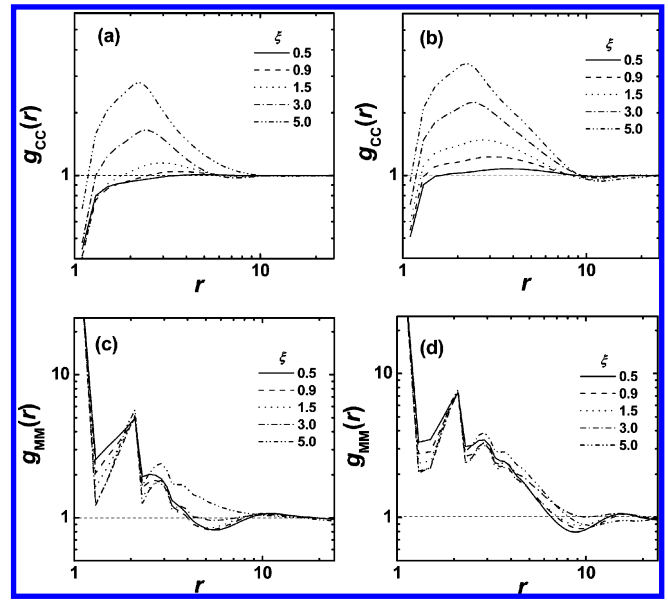

Figure 9. Counterion−counterion ($g_{CC}(r)$) and monomer−monomer ($g_{MM}(r)$) pair correlation functions for various Coulombic interaction strengths. The hydrophobic strength is set as $\varepsilon = 5$ for (a) and (c), $\varepsilon = 8$ for (b) and (d).

Based on the above results, the effect of Coulombic interaction strength on gelation can be clearly understood. For $\varepsilon = 5$, it is always in the sol state. Although increasing ξ leads to a slight increase of loop chains fraction, too weak a hydrophobic interaction is not enough to form the gel network. However, the onset of counterion condensation will screen the relatively strong Coulombic interaction, making the forming of an infinite network more possible, which is significant for $\varepsilon = 6.6$, 7.0, and 6.0. As ξ increases, at first, chains tend to extend their hydrophobic ends due to stronger electrostatic repulsion; then, the counterion condensation is triggered to screen the electrostatic repulsions with further increasing ξ. However, if ξ gets very high, e.g., $\xi = 5$, an unusual decrease of percolation probability is captured for $\varepsilon = 6.0$. This unusual behavior can be attributed to the fact that the charged monomers start to attract each other at high values of ξ. The increasing of ξ causes the counterions trapped around the charged monomers, forming a thin layer. The monomers from other chains may be drawn to this layer of counterions for compensating the Coulombic potential. This resembles the layer-by-layer assembly of op-

positely charged materials.[35] If the hydrophobic interaction is not strong enough to maintain bridge connection between bundles, this kind of electrostatic attraction will lead to a collapsed structure of chains. Namely, bridge chains will become unstable, and the forming of an infinite gel is unfavorable. Contrarily, with stronger hydrophobic interaction, the bridges are more stable and the electrostatic attraction shows no significant effects. For instance, under strong attraction ($\varepsilon = 8$), the increasing of ξ shows no significant influence on its percolation because the hydrophobic energy dominates the gelation.

4. Conclusion

In this work, simulations of telechelic polyelectrolytes in aqueous media were carried out by Monte Carlo techniques, at a very low concentration $\phi = 0.0181$ (close to the overlapping concentration ϕ^*). With a fully charged middle block and hydrophobic ends at both sides, these special polymers present novel properties compared with the neutral ones. The interplay among hydrophobic attraction, electrostatic repulsion, and counterion condensation plays an important role in the chain conformations and the forming of clusters. Different association types of chains (dangling, free, loop, and bridge) contribute to the formation of gel in different ways. In the sol state, the free type dominates and increasing hydrophobic interaction mainly leads to a transition from the free into the dangling type. However, during sol−gel transition, increasing hydrophobic interaction arouses a maximum dangling fraction due to the competition of the two transitions, the free into dangling type and dangling into bridge and loop types. In addition, the competition of hydrophobic attraction and electrostatic repulsion results in the fraction of chain conformations reaching equilibrium earlier than that of subdivided chain types. Increasing Coulombic interaction strength is basically in favor of the formation of a gel network. With increasing Coulombic interaction strength, first chains tend to extend and then collapse into loop conformation due to the screening originating from the counterion condensation layer. However, under strong hydrophobic interactions, bridge chains are more stable compared with those under small ε, and the attraction between charged monomers caused by higher ξ shows no significant effects on the percolation probability. In a word, compared with neutral gelation, the gelation of polyelectrolytes is more complicated. The association behavior of TPs will be different with varied concentrations. In fact, salt concentration is also a very important factor for the gelation behavior. All these interesting issues will be considered in our future work.

Acknowledgment. This work is supported by the National Natural Science Foundation of China (20734003) Program and the Fund for Creative Research Groups (50921062); T.S. acknowledges support from NSFC (20774096) and the Special Funds for National Basic Research Program of China (2009CB930100); Z.S. and Z.T. acknowledge support from NSFC (20534020).

Appendix: Coulombic Sum in a MC Simulation

According to the traditional Ewald method,[36] the Coulombic sum can be decomposed into two contributions: the short-ranged $\Phi_r(r_c, \alpha)$ and the long-ranged $\Phi_k(k_c, \alpha)$, where α is the Ewald parameter and controls the convergence of $\Phi_r(r_c, \alpha)$ and $\Phi_k(k_c, \alpha)$. By using error estimates,[37] some finite values of r_c and k_c are chosen to obtain $U_{elec,tot}$ at a controlled accuracy. The final expression of the Ewald potential is

$$E_{tot} = E_r + E_k + E_s + E_d \tag{A1}$$

where E_r and E_k are the contributions from the real space and the Fourier space, E_s is the self-term, and E_d is the dipole-correction term.[38] These potential terms can be written as

$$E_r = \frac{1}{2}\sum_{i,j}\sum_{\vec{n}} q_i q_j \frac{\mathrm{erfc}(\alpha|r_{ij} + \vec{n}L|)}{|r_{ij} + \vec{n}L|} \tag{A2}$$

$$E_k = \frac{1}{2}\frac{1}{\pi L^3}\sum_{\vec{k}\neq 0}\frac{4\pi^2}{k^2}\exp\left(-\frac{k^2}{4\alpha^2}\right)|\tilde{\rho}(\vec{k})|^2 \tag{A3}$$

$$E_s = -\frac{\alpha}{\sqrt{\pi}}\sum_{i=1}^{N} q_i^2 \tag{A4}$$

$$E_d = \frac{2\pi}{(1 + 2\varepsilon_s)L^3}|\sum_{i=1}^{N} q_i \vec{r}_i|^2 \tag{A5}$$

In eq A3 the reciprocal vector $\vec{k} = 2\pi\vec{n}/L$, $\vec{n} = (n_1, n_2, n_3)$: $n_t \in Z$. In eq A5 ε_s is the dielectric constant of the medium surrounding the sphere.[38] From eq A3 and eq A5 we can see that the calculation in the Fourier space and the dipole term is not pairwise additive, whereas in performing a MC move, the energy change equals the difference of the particle energy between the new and old positions. To solve the problem in MC simulation, we do the following operation. In eq A3 the square term of the Fourier-transformed charge density can be written as

$$\begin{aligned}|\tilde{\rho}(\vec{k})|^2 &= |\sum_{j=1}^{N} q_j \exp(-i\vec{k}\cdot\vec{r}_j)|^2 \\ &= (\sum_{j=1}^{N} q_j \cos(\vec{k}\cdot\vec{r}_j))^2 + (\sum_{j=1}^{N} q_j \sin(\vec{k}\cdot\vec{r}_j))^2\end{aligned} \tag{A6}$$

In the program $\sum_{j=1}^{N} q_j \cos(\vec{k}\cdot\vec{r}_j)$ and $\sum_{j=1}^{N} q_j \sin(\vec{k}\cdot\vec{r}_j)$ are stored in cossum[k_{max}] and sinsum[k_{max}], where k_{max}, determined by k_c, is the maximum number of vectors in the Fourier part. The changes in the above two summations are given by

$$\Delta\mathrm{cossum}[k_{max}] = \sum_{j=1}^{s} q_j \cos(\vec{k}\cdot\vec{r}_j^{new}) - \sum_{j=1}^{s} q_j \cos(\vec{k}\cdot\vec{r}_j^{old})$$

$$\Delta\mathrm{sinsum}[k_{max}] = \sum_{j=1}^{s} q_j \sin(\vec{k}\cdot\vec{r}_j^{new}) - \sum_{j=1}^{s} q_j \sin(\vec{k}\cdot\vec{r}_j^{old})$$

where s is the number of charged particles involved in an MC move.

Thus, the change of E_k due to the movement of the charged particles is

$$\Delta E_k \sim \sum_{\vec{k}>0} C(k)[(\Delta\text{cossum}[k] + \text{cossum}[k])^2 + (\Delta\text{sinsum}[k] + \text{sinsum}[k])^2 - (\text{cossum}[k]^2 + \text{sinsum}[k]^2)]$$
$$= \sum_{\vec{k}>0} C(k)\begin{bmatrix}2\Delta\text{cossum}[k]\ \text{cossum}[k] + 2\Delta\text{sinsum}[k]\ \text{sinsum}[k] + \\ \Delta\text{cossum}[k]^2 + \Delta\text{sinsum}[k]^2\end{bmatrix} \quad \text{(A7)}$$

where $C(k) = (4\pi^2)/(k^2) \exp(-(k^2)/(4\alpha^2))$.

For every reciprocal vector $\vec{k}$, we compute the Δcossum[k] by using the stored cossum[k] and update the latter if a MC trial is permitted. The same operation is carried out on the Δsinsum[k]. For the dipole term E_d we store the $\sum_{i=1}^{N} q_i \vec{r}_{t,i} (\vec{r}_{t,i} = (r_{x,i}, r_{y,i}, r_{z,i}))$ as dipole[t] and compute Δdipole[t] instead of the whole dipole[t]. The energy change of dipole term E_d is given by

$$\Delta E_d = \frac{2\pi}{(1 + 2\varepsilon_s)L^3} \sum_t (\Delta\text{dipole}[t]^2 + 2\Delta\text{dipole}[t]\ \text{dipole}[t]) \quad \text{(A8)}$$

where dipole[t] is updated as well as cossum[k]. Thus, the complication of E_k and E_d is reduced significantly, and this method is simple and convenient. By optimizing the Ewald parameter α, we reduce the summation in the real space to the normal minimum image convention with $\vec{n} = 0$, which is essential to increase efficiency. In fact, the self-term E_s is balanced out in the calculation, and terms like $C(k)$ can be calculated at the beginning of the simulation.

References and Notes

(1) Serres, A.; Baudys, M.; Kim, S. W. *Pharm. Res.* **1996**, *13*, 196.
(2) Bromberg, L. E.; Ron, E. S. *Adv. Drug Delivery Rev.* **1998**, *31*, 197.
(3) Yuk, S. H.; Bae, Y. H. *Crit. Rev. Theor. Drug Carrier Syst.* **1999**, *16*, 385.
(4) Qiu, Y.; Park, K. *Adv. Drug Delivery Rev.* **2001**, *53*, 321.
(5) Wittemann, A.; Azzam, T.; Eisenberg, A. *Langmuir* **2007**, *23*, 2224.
(6) Riegel, I. C.; Samios, D.; Petzhold, C. L.; Eisenberg, A. *Polymer* **2003**, *44*, 2117.
(7) He, C. L.; Kim, S. W.; Lee, D. S. *J. Controlled Release* **2008**, *127*, 189.
(8) Esquenet, C.; Terech, P.; Boue, F.; Buhler, E. *Langmuir* **2004**, *20*, 3583.
(9) Determan, M. D.; Guo, L.; Thiyagarajan, P.; Mallapragada, S. K. *Langmuir* **2006**, *22*, 1469.
(10) Kyrylyuk, A. V.; Fraaije, J. G. E. M. *J. Chem. Phys.* **2004**, *121*, 9166.
(11) Katsampas, I.; Tsitsilianis, C. *Macromolecules* **2005**, *38*, 1307.
(12) Tsitsilianis, C.; Iliopoulos, I. *Macromolecules* **2002**, *35*, 3662.
(13) Esquenet, C.; Terech, P.; Boue, F.; Buhler, E. *Langmuir* **2004**, *20*, 3583.
(14) Gotzamanis, G. T.; Tsitsilianis, C.; Hadjiyannakou, S. C.; Patrickios, C. S.; Lupitskyy, R.; Minko, S. *Macromolecules* **2006**, *39*, 678.
(15) Bossard, F.; Aubry, T.; Gotzamanis, G.; Tsitsilianis, C. *Soft Matter* **2006**, *2*, 510.
(16) Chen, C. C.; Dormidontova, E. E. *Macromolecules* **2006**, *39*, 9528.
(17) Baljon, A. R. C.; Flynn, D.; Krawzsenek, D. *J. Chem. Phys.* **2007**, *126*, 044907.
(18) Anderson, J. A.; Travesset, A. *Macromolecules* **2006**, *39*, 5143.
(19) Ortiz, V.; Nielsen, S. O.; Klein, M. L.; Discher, D. E. *J. Polym. Sci., Part B: Polym. Phys.* **2006**, *44*, 1907.
(20) Loverde, S. M.; Ermoshkin, A. V.; De La Cruz, M. O. *J. Polym. Sci., Part B: Polym. Phys.* **2005**, *43*, 796.
(21) Yuan, S. L.; Zhang, X. Q.; Xu, G. Y.; Zhang, D. J. *J. Mol. Model.* **2006**, *12*, 406.
(22) Feng, J.; Ruckenstein, E. *J. Chem. Phys.* **2006**, *124*, 124913.
(23) Jeon, J.; Dobrynin, A. V. *J. Phys. Chem. B* **2006**, *110*, 24652.
(24) Wang, Z. W.; Rubinstein, M. *Macromolecules* **2006**, *39*, 5897.
(25) Potemkin, I. I.; Vasilevskaya, V. V.; Khokhlov, A. R. *J. Chem. Phys.* **1999**, *111*, 2809.
(26) Potemkin, I. I.; Andreenko, S. A.; Khokhlov, A. R. *J. Chem. Phys.* **1999**, *115*, 4862.
(27) Gordon, H. L.; Valleau, J. P. *Mol. Sim.* **1995**, *14*, 361.
(28) Kumar, S. K.; Panagiotopoulos, A. Z. *Phys. Rev. Lett.* **1999**, *82*, 5060.
(29) Kumar, S. K.; Douglas, J. F. *Phys. Rev. Lett.* **2001**, *87*, 188301.
(30) Li, Y. Q.; Shi, T. F.; Sun, Z. Y.; An, L. J. *J. Phys. Chem. B* **2006**, *110*, 26424.
(31) Tanaka, F. *J. Non-Cryst. Solids* **2002**, *307−310*, 688.
(32) Manning, G. S. *J. Chem. Phys.* **1969**, *51*, 924.
(33) Oosawa, F. *Biopolymers* **1968**, *6*, 1633.
(34) Stevens, M. J.; Kremer, K. *J. Chem. Phys.* **1995**, *103*, 1669.
(35) Schmitt, J.; Grünewald, T.; Krajer, K.; Pershan, P.; Decher, G. *Macromolecules* **1993**, *26*, 7058.
(36) Adams, D. J.; Dubey, G. S. *J. Comput. Phys.* **1987**, *72*, 156.
(37) Kolafa, J.; Perram, J. W. *Mol. Sim.* **1992**, *9*, 351.
(38) Allen, M. P.; Tildesley, D. J. *Computer Simulations of Liquids*; Oxford University Press: London, 1987.

JP9092404